NANO · MICRO small
www.small-journal.com

Carbon Quantum Dots with Tunable Size and Fluorescence Intensity for Development of a Nano-biosensor

*So Yeon Park, Justin Kok Soon Tan, Xuancheng Mo, Yujin Song, Jiaqi Lim, Xuan Ru Liew, Hyunsoo Chung, and Sangho Kim**

Carbon quantum dots (CQDs) are a class of nanomaterials known for their remarkable photostability, chemical inertness and biocompatibility. Changing their size, structure, and surface chemistry enable the tuning of their luminescence property, which gives them tremendous potential for various applications. CQDs synthesis typically involves long tedious processes, requiring multiple steps and harsh reaction conditions. Here, a new reliable, economical, and ultra-rapid one-step fabrication method is introduced to obtain CQDs with well-defined and reproducible photoluminescence properties via a simple heat treatment. These solid-state CQDs are homogenous in size and are ready to use without the need for further purification. The size of the fabricated CQDs and their corresponding peak fluorescence intensity are confirmed to be tunable by simple adjustment of the heat treatment conditions. Coupled with their selective fluorescence quenching by metal ions, the clinical potential of CQDs is demonstrated for biosensing applications by designing a new nano-biosensor to assess the quality of stored blood units through hemolysis quantification without disrupting storage conditions. This may pave the way for a new standard in blood bank inventory management.

1. Introduction

Carbon quantum dots (CQDs) are a relatively new material class that has drawn extensive attention over the past decade. Besides their luminescence property, CQDs exhibit low toxicity, biocompatibility, photostability, and water solubility, which make them ideal for applications in bioimaging, sensing, photocatalysis, and waste water treatment.[1] To this end, substantial efforts have been made to prepare CQDs from various carbon-containing precursors by "bottom-up" and "top-down" approaches. However, these protocols typically involve long tedious processes requiring harsh reaction conditions, often demanding intermediate steps that severely complicate the synthesis process.[2] Furthermore, controlling the size of carbon nanoparticles to modulate their optical properties remains a bottleneck to realizing the full potential of CQDs with respect to their intrinsic fluorescence properties.[3] Strategies for size-differentiated synthesis of CQDs have been reported,[4] and these are similarly associated with complicated and resource-demanding methods requiring precise reagent control. Alternatively, there are approaches for separating the CQDs by size using gradient centrifugation or ultrafiltration techniques.[5] However, these separation methods are time and energy consuming, and thus have limited potential in terms of large-scale production. Therefore, it would be ideal to produce CQDs that can be homogenous in size and easily tuned for a variety of applications.[6] More importantly, conventional approaches predominantly produce CQDs suspended in solution. In comparison, a solid-state sensor is more convenient, portable and stable for point-of-care tests.[7] However, to produce a solid-state CQD sensor, tedious post-modification is required as CQDs have to be extracted, isolated from the liquid media, and bound to solid substrates.[8] Simplifying the CQDs synthesis process while achieving highly photoluminescent and photostable solid-phase CQDs without post-treatment remains a challenge.

Since carbon is ubiquitously present in all organic matter, various types of CQDs can be produced from readily accessible materials such as paper. Paper is an attractive and promising substrate material for many applications due not only to its exceptional accessibility but also to its physical properties. Its intrinsic network of randomly interwoven fibers provides a

S. Y. Park, J. K. S. Tan, X. Mo, Y. Song, J. Lim, X. R. Liew, S. Kim
Department of Biomedical Engineering
National University of Singapore
Singapore 117583, Singapore
E-mail: bieks@nus.edu.sg
J. K. S. Tan, S. Kim
N.1 Institute for Health
National University of Singapore
Singapore 117456, Singapore
J. Lim, S. Kim
NUS Graduate School for Integrative Sciences and Engineering
National University of Singapore
Singapore 119077, Singapore
H. Chung
Department of Internal Medicine and Department of Medical Device Development
Seoul National University College of Medicine
Seoul 03080, Republic of Korea
The ORCID identification number(s) for the author(s) of this article can be found under https://doi.org/10.1002/smll.202404524

© 2025 The Author(s). Small published by Wiley-VCH GmbH. This is an open access article under the terms of the Creative Commons Attribution-NonCommercial-NoDerivs License, which permits use and distribution in any medium, provided the original work is properly cited, the use is non-commercial and no modifications or adaptations are made.

DOI: 10.1002/smll.202404524

large surface area for modification and functionalization.[9] Owing to its high biocompatibility, biodegradability, disposability, and chemical/biological inertness, paper-based analytical devices have garnered significant attention in fluid handling and analysis, evident from their use in lateral flow immunoassays for pregnancy and COVID-19.[10] These properties enable paper-based devices to conform to the ASSURED criteria (Affordable, Sensitive, Specific, User friendly, Rapid and Robust, Equipment-free and Deliverable to end users) defined by the World Health Organization for point-of-care tests.[11]

In view of the usefulness of paper for biomedical applications, a few studies have demonstrated the synthesis of CQDs from paper or cellulose-based precursors. Park et al. produced color tunable CQDs from wastepaper using a solvothermal approach which yielded CQDs doped with various surface moieties.[12] Similarly, John et al. obtained amine functionalized CQDs by treating the paper substrate in an aminosilane reagent.[13] Obviating the use of any chemicals, Zhu et al. described a pyrolysis method of fabricating CQDs from plant leaves by burning for 2 h in the presence of nitrogen.[14] While these studies clearly illustrate the feasibility of deriving CQDs from paper or cellulose-based substrates, their fabrication protocols require complicated and resource-demanding steps with precise reagent control and thus are still time-consuming and labor-intensive.

Here, we report a simple ultra-rapid one-step heat treatment approach (<20 min) to synthesize luminescent CQDs using paper as the substrate precursor. Our CQDs displayed an exceptional size tunability by facile adjustment of heating parameters, yielding deterministic and stable fluorescence emission. In addition, our method produces CQDs in-situ in the solid phase, avoiding the need for subsequent separation steps to obtain a homogenous distribution of CQDs. The CQDs exhibited selective fluorescence quenching by metal ions and organic compounds via photo-induced electron transfer, which may be capitalized on to identify target analytes for biosensing applications. Leveraging on their extensive quenching by ferric iron (Fe^{3+}) and hemoglobin, we designed a CQD sensor to quantify cell-free hemoglobin (CFH) concentrations in blood. This CQD sensor showed a distinct dose-response with hemoglobin concentration, demonstrating its potential use for quality assessment of stored blood prior to transfusion. In developing the CQD sensor, we also demonstrated the optimization procedure of a new nanobiosensor.

2. Experimental Section

2.1. Chemicals and Materials

Whatman qualitative filter paper (Grade 1, GE healthcare, USA) was used as the cellulosic paper substrate in this study. Organic compounds and inorganic reagents (Sigma-Aldrich, USA) were all diluted with ultra-pure water except for cytosine, thymine, adenine, guanine, and uric acid. Cytosine and adenine were dissolved in 0.5 M hydrochloric acid while guanine in 5 M hydrochloric acid. 1 M sodium hydroxide was used as the solvent for thymine and uric acid. All chemicals and reagents were used without further purification.

2.2. Fabrication of CQDs with Tunable Fluorescence Emission

The fluorescent CQDs were prepared via a one-step heat treatment using a laboratory grade drying oven (Pol EKO Drying Oven SLN 32, Poland) with natural air convection settings. Laboratory cellulosic filter paper with a thickness of 180 µm and a pore size of 11 µm (Whatman Grade 1, GE Healthcare, Buckinghamshire, UK) was heated at 230 °C for 10 min for demonstration of CQD synthesis. For each batch 800 mg of filter paper was placed on a stainless-steel baking tray in the pre-heated oven for the required duration. To ensure even exposure to heat, the filter paper substrates were laid flat on the center rack of the oven without stacking. Subsequently, the samples were removed and allowed to cool down to room temperature prior to characterization in situ or extraction. For the parametric study on the effects of heating temperature and duration on the CQD synthesis, the heating temperature was varied from 150 to 230 °C for durations from 3 to 60 min.

2.3. Material Characterization of CQDs

Photographic images were captured with a standard digital camera (fixed ISO, exposure time, and white balance) while exposed to ambient and ultraviolet (UV) light (8W lamp, 365 nm, Spectroline EN-180 L/FBE, Spectronics Corp., USA) under dark-room conditions to qualitatively demonstrate the photoluminescence of the heat-treated paper. The fluorescence and absorbance spectra were measured using a multimode microplate reader (Spark, Tecan Group Ltd., Switzerland). The heat-treated cellulose sheets were cut into 113 mm^2 circles and loaded into a black flat 96-well plate (655900, Greiner Bio-one, Austria) for spectral characterization of the in-situ fabricated CQDs across an excitation wavelength (λ_{ex}) range of 320 to 380 nm within the emission wavelength (λ_{em}) range of 400–600 nm.

To isolate the CQDs formed in the cellulose matrix for further characterization, 800 mg of the heat-treated cellulose sheets was eluted in 4 ml of deionized (DI) water and agitated by vortex mixing for 2 min. The resulting eluent solution was filtered through a 0.22 µm microporous membrane (Minisart, Satorius, Germany) for the removal of larger cellulose fibers. The supernatants containing the CQDs were aspirated for measurement. Morphological assessments of the CQDs were performed with aberration-corrected TEM (JEOL, JEM-2100, Japan) operating at 80 kV acceleration voltage. For elemental analysis, Fourier transform infrared (FTIR) spectra were collected using a FTIR spectrometer (Nicolet iS50, Thermo Scientific, USA) in attenuated total reflection mode in the range of 400–4000 cm^{-1} while X-ray photoelectron spectra (XPS) were measured using a conventional spectrometer (ESCALAB Xi+, ThermoFisher, USA). 13C NMR spectroscopy (Agilent-NMR-vnmrs600, Agilent, USA) was performed using dimethyl sulfoxide–D6 as the solvent. Raman spectra were recorded on a laser Raman spectrometer (Horiba, HR Evolution, Japan) with an excitation wavelength of 633 nm.

© 2025 The Author(s). Small published by Wiley-VCH GmbH

UV photoelectron spectroscopy was conducted with a monochromatic He I light source (Shimadzu, UV3600 Plus, Japan). Dynamic light scattering was performed with a Zetasizer (Nano ZS ZEN 3600, Malvern, UK).

2.4. Blood Sample Preparation and Hemoglobin (Hb) Measurement

This study was approved by the National University of Singapore Institutional Review Board (H-18-006) and all procedures were performed in accordance with the approved guidelines. Healthy male volunteers aged between 21 and 40 years old, without any known pathological conditions, were recruited. Informed consent was obtained from all recruited participants. All blood collection and storage processes were performed under sterile conditions. Whole blood (20 ml) was collected from the donors into vacutainer tubes with citrate-phosphate-dextrose (Terumo, Japan) in the ratio of 7:1. The blood sample was then centrifuged at 2000 x *g* for 10 min at 4 °C (Sigma 2–6, Germany) to remove the plasma and buffy coat. The top 2 mm layer of the packed red blood cells (RBCs) was also removed to minimize the presence of leukocytes. To examine the effect of storage duration and its effect on hemolysis, the packed RBCs were resuspended in saline–adenine–glucose–mannitol (SAGM) additive solution (Terumo, Japan) to hematocrit of 60 – 70% and stored under standard blood banking conditions (2 – 6 °C). Hematocrit was measured with a microhematocrit centrifuge (Sigma 1–14 Microcentrifuge, Sartorius AG, Germany). The RBC samples were aliquoted aseptically for measurements on Days 0, 1, 14, 28, 42, and 49. The aliquoted samples were centrifuged at 2500 x *g* for 10 min at 4 °C to separate the storage media from the packed RBCs. The extracted supernatant was then used to measure CFH levels with a commercially available biochemical assay (MAK115, Sigma-Aldrich, USA) and our CQD sensor. Total Hb was quantified by the cyanmethemoglobin method using a blood analyzer (HemoCue Hb 301, Sweden). For validation of our sensor performance, 10 µl of the extracted storage media was loaded onto our in-situ CQDs and dried at 70 °C for 10 min before Hb measurement.

2.5. Statistical Analysis

Data visualization and statistical analysis were performed with Origin 2019b (OriginLab, USA). Results are presented as mean ± standard deviation (SD). Unpaired Student's t-test (for parametric samples) and one-way ANOVA (for non-parametric samples) were used to analyze the data. Differences were considered statistically significant for $P < 0.05$.

3. Results

3.1. In-Situ Formation of CQDs on Paper

We invented a one-step ultra-rapid method for fabrication of in situ CQDs with deterministic sizes and tunable fluorescence emission (**Figure 1a**). The heat treatment carbonized the cellulose fibers, increasing the peak fluorescence intensity (FI) of the cellulose fivefold (Figure 1b). Both the heating temperature and duration were found to contribute to the tunability of the peak FI (Figure 1c). The fluorescence of the CQDs was observed under both visible and UV light conditions. The heat-treated cellulose displayed visible photoluminescence when exposed to UV light with an excitation wavelength (λ_{ex}) of 365 nm (Figure 1d). The CQDs extracted in DI water exhibited photoluminescence when illuminated by UV light (Figure 1e), which is attributed to the intrinsic band edge and electron hole recombination in the sp^2 cluster.[15] This photoluminescence exhibited a clear λ_{ex} dependence of the emission wavelength (λ_{em}) and intensity,[16] which is a typical optical property of CQDs.[17] The fluorescence spectra of the CQDs derived from a λ_{ex} sweep showed a maximum FI at an excitation of 365 nm with a peak λ_{em} of 428 nm. The peak FI at λ_{ex} = 365 nm exhibited a red shift (12 nm) with ~200% enhancement as compared to CQDs excited at 320 nm. Subsequent increments of λ_{ex} resulted in a reduction of FI peak (≈78%) and a further red shift (22 nm) (Figure 1f). This has been identified as a generic feature of CQDs, suggesting that these particles could possess multiple FI centers resulting from either different conjugation length of the carbon core or various surface functional groups.[18] Conventional CQDs with higher oxidation degrees exhibit λ_{ex} dependence of their FI properties over the wavelength range of 280 – 380 nm,[19] which coincides with the peak λ_{ex} of 365 nm for our CQDs. The shift in emission peak positions with different excitation wavelengths is attributed to the different emissive sites on CQDs.[20] At different excitation wavelengths, specific corresponding emissive sites would be excited and fluoresce, resulting in an excitation-dependent behavior of emission spectra.

3.2. Morphological and Structural Characteristics of CQDs

To characterize the morphology of the in-situ CQDs, dynamic light scattering (DLS), transmission electron microscopy (TEM) and high-resolution transmission electron microscopy (HRTEM) were utilized. DLS yielded a size distribution within the range of 2.33 – 3.62 nm, with an average diameter of 2.94 ± 0.48 nm (Figure 1g). To distinguish the presence of cellulosic fiber from the CQDs formed, both cellulose (non-heat treated) and in-situ CQDs on cellulose were observed under TEM. As seen from the TEM images, cellulose appeared as distinct fiber-like structures (Figure 1h) while CQDs were shown to be visible dark round spots (Figure 1i). Quantitative analysis of the TEM images also revealed that the CQDs were homogenous and monodispersed with a mean particle diameter of 3.13 ± 1.06 nm. The HRTEM images illustrated the high crystallinity structure of CQDs with similar well-resolved lattice fringes (Figure 1i **inset**). The crystal plane spacing of 0.21 nm corresponds to the (100) graphite plane, which is often observed in CQDs.[21] Overall, the obtained size distribution was in good agreement with previously reported CQD dimensions (1 – 10 nm),[22] confirming the presence of CQDs in the cellulose matrix.

3.3. Photoluminescence Characteristics of CQDs

To investigate the origin of the observed photoluminescence, the fluorescence excitation and absorption spectra of cellulose and

© 2025 The Author(s). Small published by Wiley-VCH GmbH

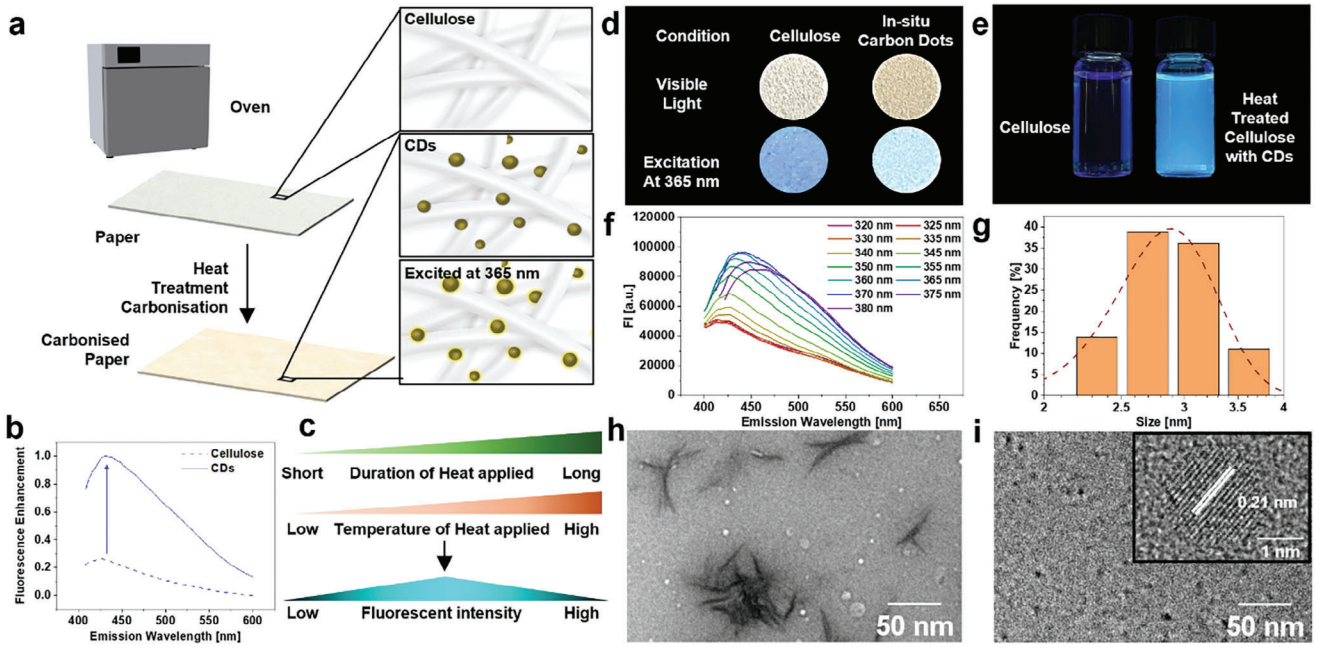

Figure 1. Synthesis and characterization of CQDs. a) Schematic illustration showing the one-step fabrication process of producing in-situ CQDs on paper. b) Fluorescence enhancement was observed after heat treatment (dotted and solid lines represent cellulose and in-situ CQDs on paper, respectively). c) Temperature and duration dependence of the FI of in-situ CQDs. d) Photographs of heat-treated cellulose paper under visible and UV illumination. e) Isolated CQDs in solution form under UV light exposure in dark room conditions. f) FI spectra of the CQDs under different excitation wavelengths. g) Size distribution of extracted CQDs with gaussian fit (dotted line). h) TEM image showing extracted non-heat-treated cellulose fibers. i) TEM image showing extracted CQDs (inset: HRTEM image of extracted CQD with clear lattice fringes).

in-situ CQDs on cellulose were measured by spectrophotometry. As expected, the CQDs showed stronger optical absorption in the UV region (260 to 320 nm),[23] which is produced by the transition of the valence electron energy ($\pi - \pi^*$ and $n - \pi^*$ transitions).[24] The UV–vis absorption spectrum of our CQDs (**Figure 2a**) showed an absorbance band at 264 nm, which corresponds to the $\pi - \pi^*$ transitions of aromatic sp^2 domains in the C=C bonds present in CQDs fabricated at higher temperatures as a result of the quantum confinement effect;[25] which was absent in the solutions extracted from non-heat treated cellulose samples. Conventional CQDs previously reported showed similar results with a typical absorption peak in the region of 250 to 300 nm, representing the typical absorption of an aromatic π system.[26]

The in situ CQDs exhibited the same stretching vibration bands in their FTIR spectra (Figure 2b) in comparison to non-heat-treated cellulose. The peak at 3315 cm^{-1} can be attributed to OH stretching vibrations, indicating the existence of carboxyl and hydroxyl groups, which allows good water solubility and long-term stability.[17] The absorption band present at 2889 cm^{-1} (alkanes stretching) indicates C—H bonds. The peak at 1631 cm^{-1} represents C=C double bonds in an aromatic ring.[27] Further carboxyl groups are confirmed by the small peak at 1024 cm^{-1}, assigned to C—O stretching vibrations.[28] Smaller absorption bands at 892, 1109 and 1155 cm^{-1} are attributed to group C frequency, ring asymmetric stretching, C—O-C asymmetric stretching, respectively.[29] The obtained FTIR spectrum was in agreement with the previously reported cellulose pulp spectrum.[29] The cellulose and heat-treated cellulose share the same FTIR bands, thus revealing similar functional groups present on the surface of CQDs. Elemental composition and carbon bonding configurations of the CQD surface were measured by XPS (Figure 2c). The high resolution C1s XPS spectrum (Figure 2d) shows 3 peaks at 283.0, 284.7, and 286.1 eV, which correspond to C=C, C—C, C—O, respectively.[30] The O1s XPS spectrum (Figure S1, Supporting Information) contains one peak at 532.5 eV which stems from the C—O previously identified.[22] Thus, the XPS results further corroborate the conclusion of the FTIR data. Raman spectra (Figure 2e) was used to identify the state of carbon of CQDs, which showed typical peaks present in the region between 1095 and 1122 cm^{-1} attributed to the axial deformation of C—O[31] and which coincide with previously reported cellulose bands.[32] Nuclear magnetic resonance (NMR) spectroscopy (13C) was used to determine functional groups on the surface of the CQDs (Figure 2f). Signal peaks below and above 90 ppm indicate the presence of both aliphatic and aromatic carbons. The observed signals in the range of 50 to 80 ppm show the existence of aliphatic sp^3 carbons and carbons attached with hydroxyl groups,[33] which is consistent with the FTIR results. Separately, the observed signals within 80 to 100 ppm are assigned to aromatic sp^2 carbons attached with ether linkages. In addition, our CQDs demonstrated astounding photostability when kept in the dark with a FI for a prolonged duration at room temperature (25 °C) (Day 0: 33006.75 ± 703.30, Day 42: 33657 ± 1031.34, $p = 0.087$, $n = 12$) (Figure 2g).

We investigated the interaction of the CQDs with both metal ions and organic compounds to check for their chemical reactivity. Due to the presence of multiple functional groups on the

 © 2025 The Author(s). Small published by Wiley-VCH GmbH

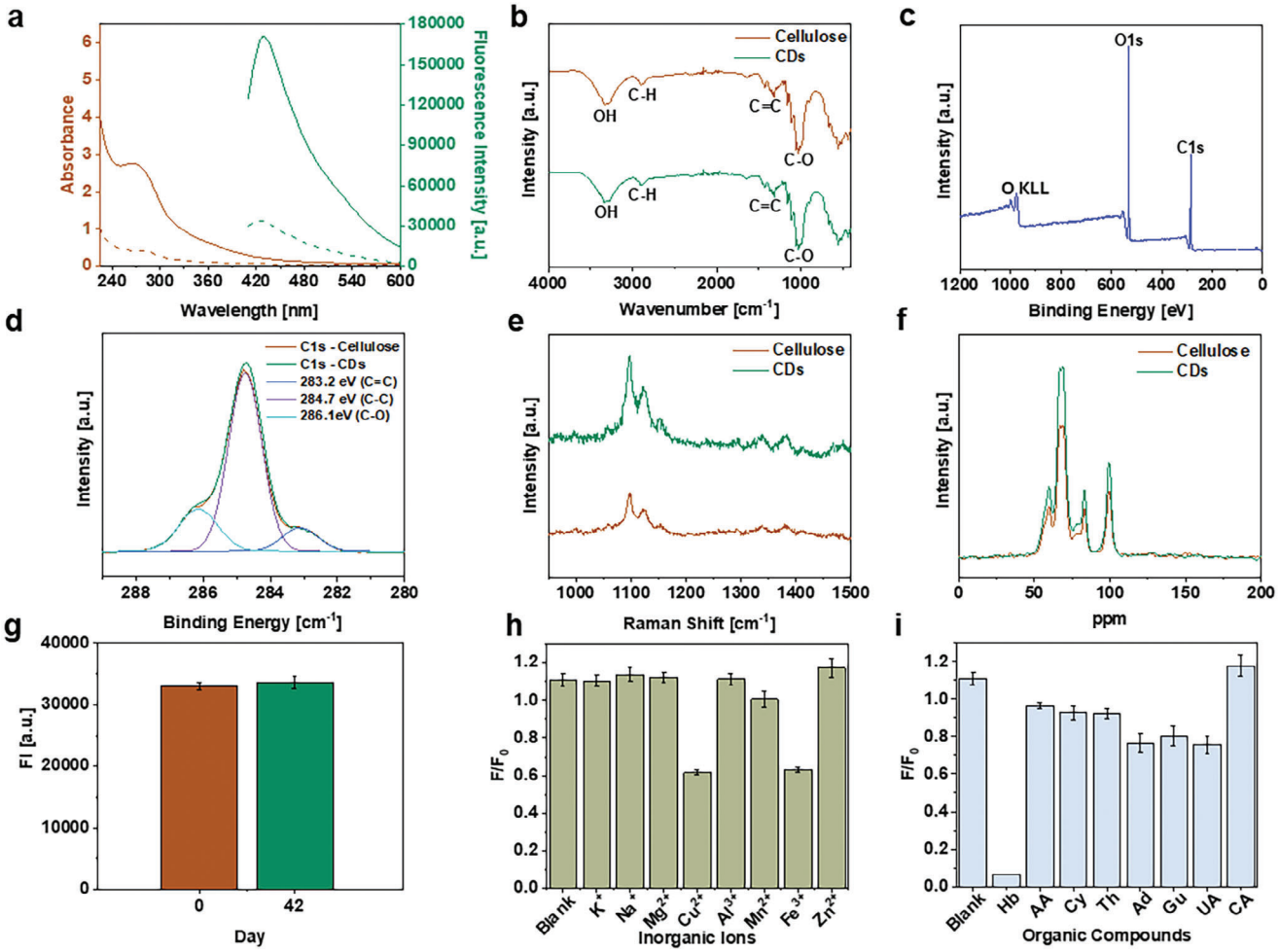

Figure 2. Spectrophotometric analysis and fluorescence stability of CQDs. a) Fluorescence spectra (green) of cellulose and CQDs with excitation at 365 nm and the corresponding absorption spectra (orange) of the extracted cellulose and CQDs (CQDs: solid line, Cellulose: dotted line). b) FTIR spectrum of cellulose and CQDs. c) XPS survey spectrum of CQDs. d) High-resolution C1s XPS spectrum of cellulose and CQDs. e) Raman spectroscopy identifying the proportion of sp^2 and sp^3 hybridized carbon atoms in the carbon core of cellulose and CQDs. f) 13C NMR spectra of cellulose and CQDs. g) Photostability of CQDs kept in the dark at 25 °C. h,i) Normalised FI of CQDs in the presence of various inorganic ions (h) and organic compounds (i).

surface of the CQDs, substances such as metal ions and organic compounds can interact with these groups to modulate the CQD fluorescence.[34] A representative panel of eight cations (sodium Na^+, potassium K^+, aluminium Al^{3+}, iron Fe^{3+}, copper Cu^{2+}, zinc Zn^{2+}, magnesium Mg^{2+}, and manganese Mn^{2+}), each at a concentration of 1 mM, was selected to evaluate their effects on the CQD fluorescence.[35] The normalized fluorescence of the CQDs (F/F_0, where F_0 and F are the FI of the in-situ CQDs before and after the loading of inorganic ion samples, respectively) were significantly quenched by Cu^{2+} and Fe^{3+} while other ions exerted negligible effects (Figure 2h). The selective fluorescence quenching of CQDs by the metal ions is due to the strong binding energy between the ions and the electron-rich oxygen groups on the surface of CQDs.[36] This quenching effect may be attributed to the formation of stable complexes with Cu^{2+} and Fe^{3+} ions through the surface carboxyl and hydroxyl groups that have high binding affinity for these ions,[37] alluding to the potential of our CQDs to be used as nano-sensors for measuring Cu^{2+} and Fe^{3+} in human body fluids. To test the feasibility of this, organic compounds (Hemoglobin (Hb), Ascorbic Acid (AA), Cytosine (Cy), Thymine (Th), Adenine (Ad), Guanine (Gu), Uric Acid (UA), and Citric Acid (CA)), each at a concentration of 1 mM, were also added to the CQDs.[38] The results showed that the fluorescence of CQDs was strongly quenched in the presence of iron-containing Hb, corroborating the quenching by Fe^{3+} (Figure 2i). These results demonstrate the possibility of extrapolating the biosensing applicability to various other target analytes.

3.4. Tunability of peak FI

To better understand the formation of CQDs on paper, the effect of heating duration and temperature on the carbonization process were systematically investigated. We hypothesized that the formation of the fluorescent compounds could be controlled by adjusting the heating dose. As such, cellulose sheets were heat-treated at different temperatures and durations, which yielded CQDs with different peak FIs and sizes. First, the cellulose was

© 2025 The Author(s). Small published by Wiley-VCH GmbH

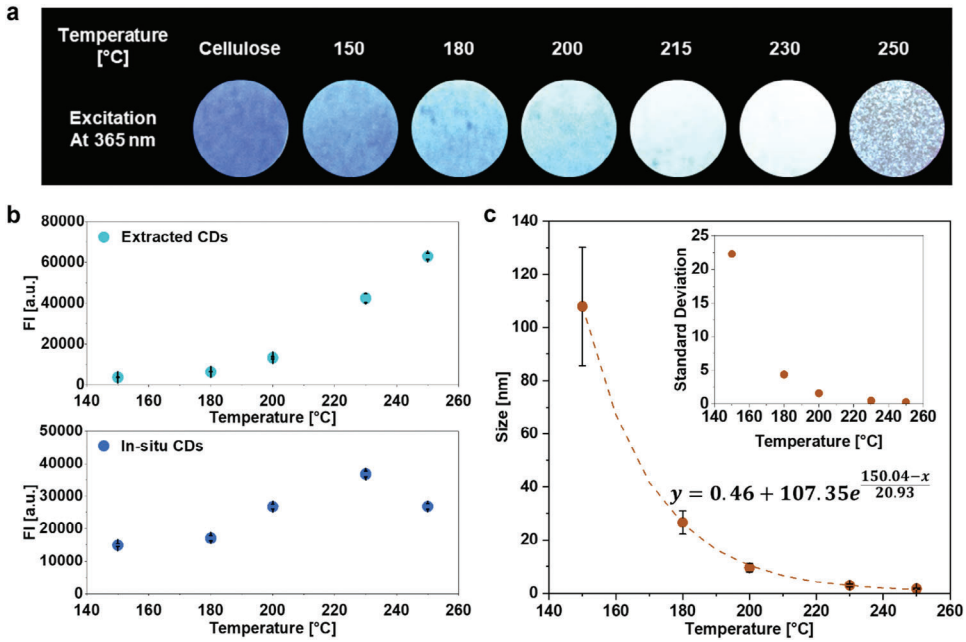

Figure 3. Temperature-dependent FI tunability of in-situ CQDs. a) Images of heat-treated cellulose paper under UV light for different heating temperatures (150 °C to 250 °C) with a fixed duration of 10 min. b) Peak FI of CQDs fabricated with different temperatures (top: Extracted CQDs, bottom: In-situ CQDs). c) Relationship between CQD size and treatment temperature (inset: Standard deviation of CQD size).

heated at different temperatures (150, 180, 200, 230, and 250 °C) for a fixed duration of 10 min. All the CQDs exhibited a maximum λ_{ex} at 365 nm regardless of the heating temperature (Figure S2, Supporting Information). Notably, the photoluminescence of the in-situ CQDs increased with temperature up to 230 °C, beyond which excessive carbonization of cellulose structure was apparent from the visible non-fluorescing brown spots on the cellulose sheet that attenuated their overall photoluminescence (**Figure** 3a). With increasing carbonization, the substrate showed a clear increase in char formation and a marked elevation in surface porosity, which would have reduced the amount of material available for CQD formation (Figure S3, Supporting Information). The peak FI of extracted CQDs displayed a monotonic increase with heating temperature to a maximum of 63032 ± 1615 a.u. at an λ_{em} of 428 nm, with no corresponding red shift (Figure 3b **top**). In contrast, the peak FI of in-situ CQDs showed a maximum at 230 °C and subsequent increase in temperature to 250 °C resulted in a drop in FI (~1.3 times drop from the maximum) (Figure 3b **bottom**). The maximum λ_{em} was 428 nm for all the treatment conditions except for the CQDs fabricated at 250 °C which exhibited a peak fluorescence red shift (12 nm) (Figure S2e, Supporting Information). The difference in FIs of the in-situ and extracted CQDs suggests that the thermal decomposition at high temperatures could lead to excessive cellulose carbonization represented by the visible brown dots formed.[39] This requires a balance between the antagonistic effects of CQD formation and cellulose carbonization to maximize the net FI of the in-situ CQDs on paper. Characteristic absorbance bands were identified at 264 nm for CQDs fabricated at 180 – 250 °C (Figure S4, Supporting Information). The increase in the absorbance peak with FI further supports the π – π^* transition as the source of the fluorescence. The DLS results revealed that the size (150 °C: 108.00 ± 22.29 nm, 180 °C: 26.57 ± 4.34 nm, 200 °C: 9.51 ± 0.48 nm, 230 °C: 2.94 ± 0.48 nm, 250 °C: 1.63 ± 0.27 nm) of the CQDs decreases exponentially with temperature ($R^2 = 0.99$) (Figure 3c), and the CQDs fabricated at higher temperatures had narrower size distributions ($SD_{150\,°C}$ = 22.29, $CV_{150\,°C}$ = 20.64% and $SD_{250\,°C}$ = 0.27, $CV_{250\,°C}$ = 16.35%) (Figure 3c **inset**). While the size distribution was comparable to previously reported CQDs that had average diameters of 3.4 ± 0.8 nm (CV = 23.52%)[40] and 5 ± 2 nm (CV = 40%),[41] we could obtain CQDs with a narrow size distribution without any post-hoc separation processes needed in conventional methods, thus greatly improving the preparation efficiency. The TEM images confirmed that the CQDs became more uniform in size when fabricated at higher temperatures (Figure S5a, Supporting Information). The CQDs were further examined by HRTEM, which revealed a lattice spacing of 0.21 nm (Figure S5a, Supporting Information inset) consistent regardless of temperature applied. Based on the heating temperature results, we selected 230 °C for the following heating duration study.

Similarly, to study the effect of heating duration on the CQD fabrication, the cellulose was heated at 230 °C for five different durations (3, 5, 10, 30, and 60 min). All CQDs showed peak emissions at the λ_{ex} of 365 nm regardless of heating duration (Figure S6, Supporting Information). With UV light exposure, the photoluminescence of the in-situ CQDs increased with the heating duration up to 10 min. Subsequently, excessive carbonization of the paper substrates resulted in clear brown spots which reduced the brightness of the fluorescence (**Figure** 4a). As expected, the peak FI of the extracted CQDs increased with heating duration, reaching a maximum at 60 min (73363 ± 803 a.u.) at an λ_{em} of 428 nm (Figure 4b **top**). However, the peak FI of in-situ CQDs exhibited a maximum at 10 min, after which FI dropped at 30 min (≈50%

© 2025 The Author(s). Small published by Wiley-VCH GmbH

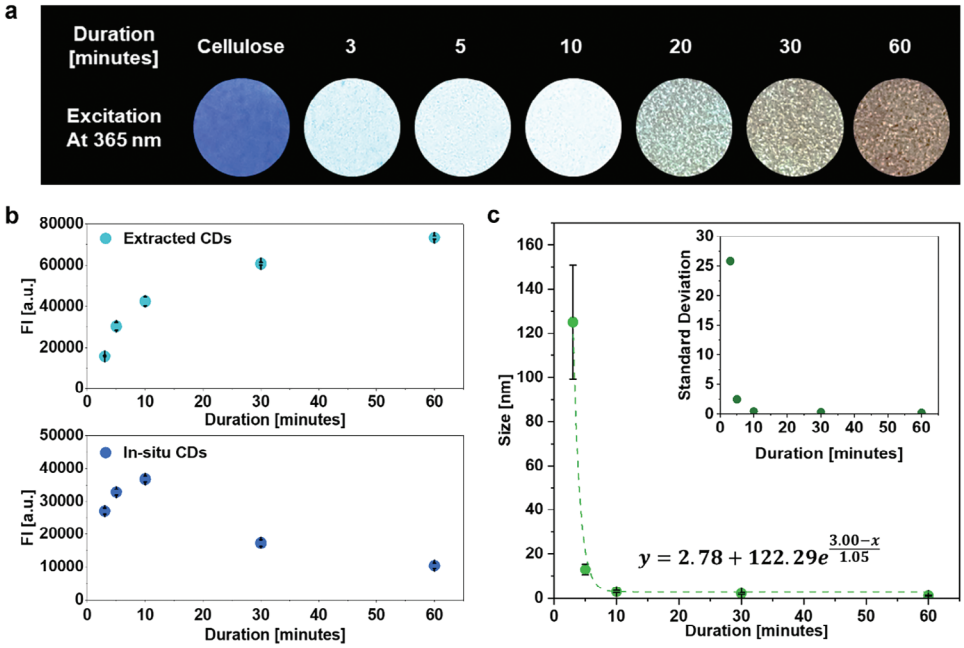

Figure 4. Heating duration-dependent FI tunability of in-situ CQDs. a) Images of heat-treated cellulose paper under UV light for the different heating durations (3–60 min) with a fixed temperature of 230 °C. b) Peak FI of CQDs fabricated with different durations (top: Extracted CQDs, bottom: In-situ CQDs). c) Relationship between CQD size and treatment duration (inset: Standard deviation of CQD size).

drop from the maximum) and 60 min (~70% drop) (Figure 4b **bottom**). An absorbance band (Figure S7, Supporting Information) was identified at 264 nm for all cellulose that was heat-treated regardless of heating duration, arising from the charge transfer between π and π^* energy levels as described above. The DLS results demonstrated a reduction in size with heating duration (3 min: 125.07 ± 25.82 nm, 5 min: 12.99 ± 2.47 nm, 10 min: 9.51 ± 0.48 nm, 30 min: 2.94 ± 0.48 nm, 60 min: 1.63 ± 0.27 nm) following an exponential decay profile (R^2 = 0.99) (Figure 4c). The CQDs fabricated beyond 5 min showed narrower size distributions ($SD_{3\ min}$ = 25.81, $CV_{3\ min}$ = 20.64% and $SD_{60\ min}$ = 0.17, $CV_{60\ min}$ = 16.34%) (Figure 4c **inset**). Similar to the heating temperature, the TEM images showed that the CQDs size distributions were more homogenous at longer durations (Figure S5b, Supporting Information). HRTEM images also confirmed that the CQDs had a lattice spacing of 0.21 nm (Figure S5b, Supporting Information **inset**) which persisted regardless of the heating duration, corresponding to the (100) graphite plane. In both the FTIR and XPS spectra, identical bands were found regardless of the treatment temperature (Figure S8, Supporting Information) and duration (Figure S9, Supporting Information) used to fabricate the CQDs, which demonstrate that the observed difference in FI is not due to changes in the derived products.

3.5. Design of Nano-Biosensor

We have demonstrated that in the presence of Fe^{3+} ions (Figure 2g), the FI of the CQDs decreases due to quenching arising from photo-induced electron transfer from the CQDs to the iron atom. In addition, as shown in Figure 2h, hemoglobin (Hb, an iron-containing metalloprotein) had the strongest ability to quench the fluorescence. We exploited this finding to evaluate the feasibility of using the in-situ CQDs for detecting CFH in blood bags produced as a result of the storage lesion (**Figure 5**a). To validate the clinical potential of the CQD sensor, we selected both physiological (6 – 34 mg L^{-1})[42] and pathophysiological levels (34 – 87 mg L^{-1})[43] for the test. The CQDs fabricated under different heating conditions (150 °C, 180 °C, 200 °C, and 230 °C; all for 10 min) were assessed for their CFH detection performance. As these CQDs possessed different baseline fluorescence, we sought to identify the optimal baseline FI to detect the low concentrations of CFH without FI saturation. As expected, the FI decreased with CFH concentration, and CQDs fabricated at 200 °C showed the best linear relationship (R^2 = 0.92) (Figure 5b). The sensitivity of the different fluorescence baseline conditions to CFH was quantified using the gradient of the fitted linear regression lines. The CQDs fabricated at 200 °C also showed the highest sensitivity (−48.21 ± 4.02 FI mg^{-1} L^{-1}) (Figure 5c). Collectively, CQDs fabricated at 200 °C for 10 min were demonstrated to be best suited for CFH measurement.

To better understand the quenching mechanism of CFH, the absorbance (for CFH) and FI (for CQDs and CFH) were measured separately (Figure 5d). No overlap was observed between the maximum absorption band of CFH (416 nm) and the FI emission band of CQDs (428 nm). Additionally, the FI emission band of CFH (468 nm) did not coincide with CQDs nor CFH absorbance. This suggests that the quenching mechanism was primarily based on the binding effects of CFH-CQDs, causing the photo-induced electron transfer from the C=C on the CQDs to the heme group in CFH.[44] The fluorescence spectra of in-situ CFH-CQDs samples (Figure 5e) demonstrated a monotonic decrease in peak intensity with Hb concentration, showing a peak emission band at 428 nm (CQD emission band). The time

© 2025 The Author(s). Small published by Wiley-VCH GmbH

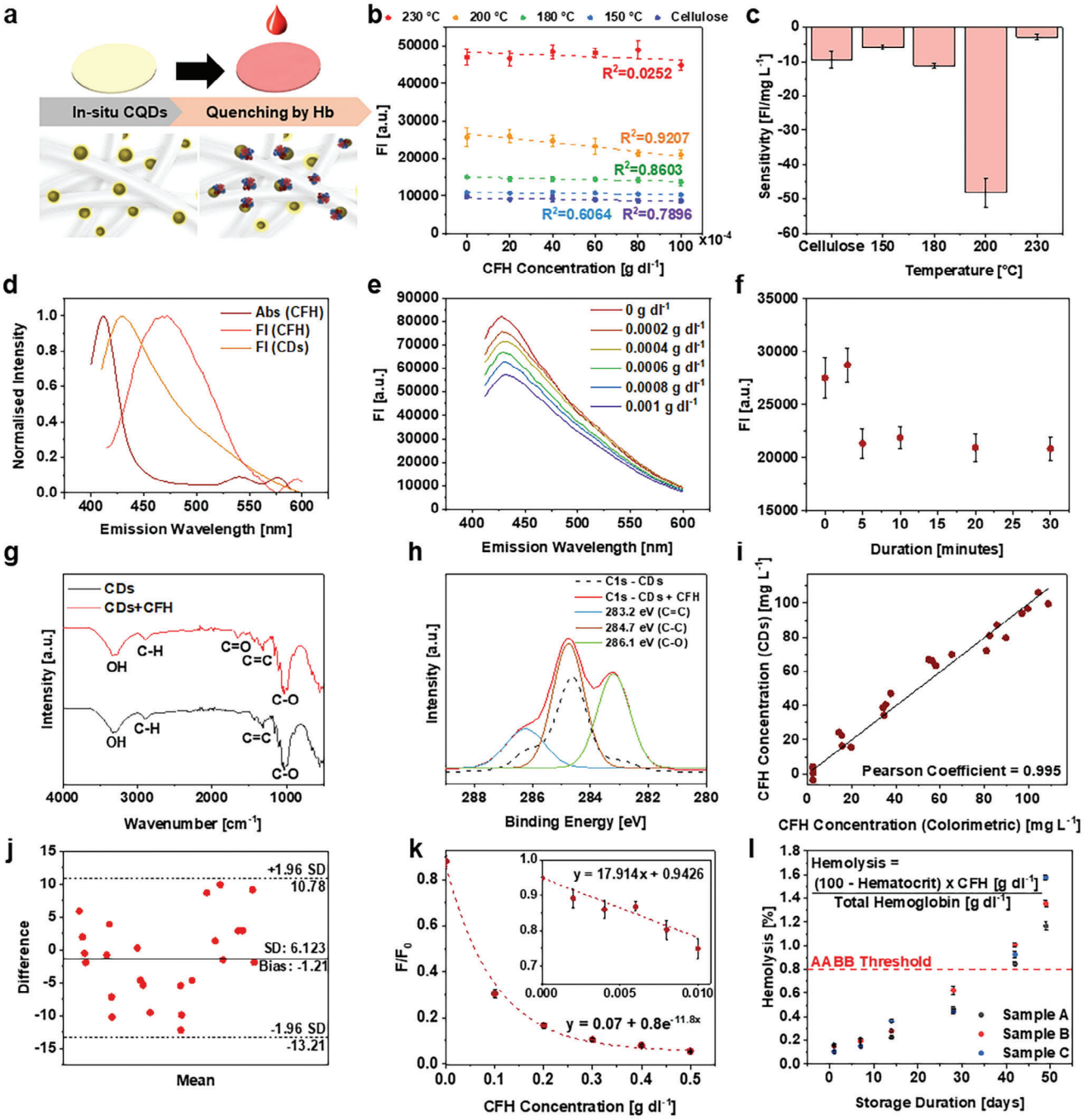

Figure 5. Detection of CFH with in-situ CQDs on paper. a) Schematic illustration showing the concept of detecting CFH concentration with CQDs. b) Quenching response curves for CQDs fabricated at different temperatures with varying baseline fluorescence intensities. c) Sensitivity of CQDs in detecting CFH. d) Fluorescence spectrum of CQDs and Hb excited at 365 nm compared against the absorbance spectrum of Hb. e) Fluorescence spectra of CFH-CQDs at different concentrations of CFH. f) Relative photoluminescence intensity of CFH-CQDs complex after CFH loaded at 365 nm excitation. g) Surface chemical groups of CFH-CQDs complex. h) High-resolution C1s XPS spectrum of the CQDs with CFH. i) Correlation analysis of measuring CFH with CQDs against colorimetric method. j) Bland Altman plot for validation of CQDs against the colorimetric method. k) Calibration plot of F/F_0, where F and F_0 are the fluorescence intensities at 365 nm excitation before and after adding CFH (inset: Calibration plot of CFH at lower concentrations of 0 – 100 mg L^{-1}). l) Quantification of hemolysis levels in blood bags during storage.

© 2025 The Author(s). Small published by Wiley-VCH GmbH

required to quench CQDs was investigated using a CFH concentration of 0.1 g dl^{-1}. Quenching of the CQDs FI saturated within 5 min after addition of CFH, indicating that the CFH-CQDs binding completes rapidly within 5 min (Figure 5f). To gain further insight into the FI quenching mechanism, the surface functional groups present on the in-situ CFH-CQDs samples were analyzed with FTIR and XPS. FTIR showed nearly identical bands in in-situ CQDs and in-situ CFH-CQDs samples (Figure 5g). The characteristic absorption band of O—H (3328 cm^{-1}) and stretching vibration band of C—O (1024 cm^{-1}) were distinctly observed, confirming the presence of carboxylic groups.[45] In addition, two absorption peaks at 2901 and 1314 cm^{-1} were found, associated with the stretching and bending vibrations of C—H and C═C, respectively.[46] A new peak was found at 1651 cm^{-1} in the CFH-CQDs complex that corresponds to the stretching vibration band of C = O, indicating the presence of -COOH group contributed by the CFH.[47] The C1s XPS spectrum (Figure 5h) of CFH-CQDs showed three peaks at 283.2, 284.7, and 286.1 eV for C═C, C—C, and C—O, respectively,[30] which is identical to CQDs. However, higher intensity was found at all 3 peak positions, due to the presence of the bound Hb.

To validate the CQD sensor for CFH detection, Hb standard solutions were serially diluted to yield a wide range of CFH concentrations found in both physiological and pathophysiological conditions. The CFH concentration was determined using the laboratory reference colorimetric method (n = 24) in parallel with our CQD sensor (n = 24). Our CQD results were in good agreement with those obtained using the conventional method, with a strong linear correlation between the two methods (Pearson correlation coefficient = 0.995) (Figure 5i). Bland-Altman analysis (Figure 5j) showed a mean bias of -1.21 mg L^{-1} with a SD of 6.12 from the conventional method. The upper and lower limits of agreement were 10.78 and -1.96 mg L^{-1} respectively, with 95% of the CFH measurements falling within the agreement limits,[48] validating the accuracy of our CQD sensor. To test if the CQDs are capable of quantifying the low amount of storage lesion-induced hemolysis in blood bags, FI quenching was measured at low CFH concentrations (0.1 – 0.5 g dl^{-1}) corresponding to hemolysis (< 1%).[49] The normalized fluorescence displayed an exponential decay with increasing CFH concentration ($F/F_0 = 0.07 + 0.8e^{-11.8[CFH]}$, $R^2 = 0.998$) (Figure 5k). The linear detection range was determined to be from 0 to 0.01 g dl^{-1} ($F/F_0 = -17.91[CFH] + 0.94$, $R^2 = 0.929$) (Figure 5k **inset**). The limits of detection and quantification (LOD and LOQ) were determined to be 0.006 and 0.021 g dl^{-1}, respectively (n = 6), based on the following formula: $LOD = 3 \times SD_{DI}$ and $LOQ = 10 \times SD_{DI}$, where SD_{DI} is the standard deviation of the [CFH] measurements for the blank (DI water) samples. The calibration curve was used to monitor changes in CFH concentration during blood storage (n = 3). The CFH level in all 3 subject samples was found to increase with the storage duration (Figure 5i). The mean CFH concentration increased from 0.08 ± 0.02 g dl^{-1} (Day 1) to 0.47 ± 0.02 g dl^{-1} (Day 42). Statistically significant increases in the CFH concentration were found at each time point of measurement ($P < 0.05$). The total Hb levels of all units ranged from 16.2 – 23.83 g dl^{-1} and decreased to a minimum at Day 49 across all subjects (19.84 ± 0.65 g dl^{-1}, $P < 0.05$). The average hematocrit of the stored blood samples decreased from 61.55 ± 0.75% (Day 1) to 55.11 ± 1.40% (Day 49), confirming a significant amount of hemolysis ($P < 0.05$) during the storage (Figure S10, Supporting Information). Our findings indicated that with prolonged storage, there was an accumulation of CFH in the storage medium, coinciding with a decrease in both the hematocrit and total Hb concentration in the stored unit.[49] Thus, we were able to quantify the degree of hemolysis within the stored blood samples during prolonged storage, which could be determined by comparing the measured CFH concentration to the total Hb concentration and hematocrit. According to blood banking guidelines set out by the Association for the Advancement of Blood and Biotherapies (AABB), the hemolysis level of RBCs at the point of transfusion must be lower than 0.8% to ensure that no hemolytic products are transfused to patients.[50] Hemolysis levels present in all three samples remained within the acceptable range (< 0.8%) up to Day 28 (Subject A: 0.46 ± 0.02%, Subject B: 0.62 ± 0.03%, Subject C: 0.44 ± 0.02%) but surpassed the threshold at Day 42 (Subject A: 0.84 ± 0.01%, Subject B: 1.01 ± 0.02%, Subject C: 0.93 ± 0.03%) (Figure 5l), which coincided with hemolysis levels found in another blood storage study.[51]

4. Discussion

Although CQDs have inherent advantages as a new class of nanomaterials, the large number of fabrication parameters adds complexity to explaining the origin of CQDs' astounding optical properties. These properties strongly depend on the synthesis conditions such as the chosen precursors, starting materials, duration, and temperature of synthesis. The top-down approach that we adopted for the CQDs fabrication involves the carbonization of larger cellulosic structures present in paper into CQDs through a simple oven-based heat treatment that permits facile fluorescence tunability of the extracted CQDs by adjusting the heating temperature and duration. Utilizing a non-cytotoxic, low-cost starting material (paper), coupled with a standard oven with low energy-consumption (13 W), we circumvent the limitations of conventional synthesis methods that require harsh conditions and high energy sources,[24] resulting in a costly and time-consuming fabrication of CQDs. CQDs are known to undergo self-quenching in solid-state form due to its aggregation and $\pi - \pi$ stacking interactions.[52] This limits the use of CQDs, particularly in sensors that typically require materials fluorescing in the solid state.[53] Our approach condenses the fabrication and embedment into a one-step in-situ formation of CQDs in the cellulosic structure. The immobilization of the CQDs in the cellulose matrix resolves the quenching problems in solid phase CQDs as coupling the CQDs with the cellulose substrate restricts the intermolecular motions.[54]

The fabrication strategy relies on the carbonization of cellulosic structure through energy transfer, which is governed by the heating temperature and duration in the oven. Heat-based synthesis methods have been used mainly as a cost-efficient route for fabrication of CQDs through saccharides, amines, organic acids and their derivatives.[55] When such products undergo heat treatment, its product phases and compositions can be empirically controlled by reaction conditions, particularly heating rates, temperature and duration.[56] Cellulose is the major component found in paper, and cellulose depolymerization begins at the temperature between 100 – 150 °C.[57] The thermal degradation of the cellulose is a complex process involving multiphase

© 2025 The Author(s). Small published by Wiley-VCH GmbH

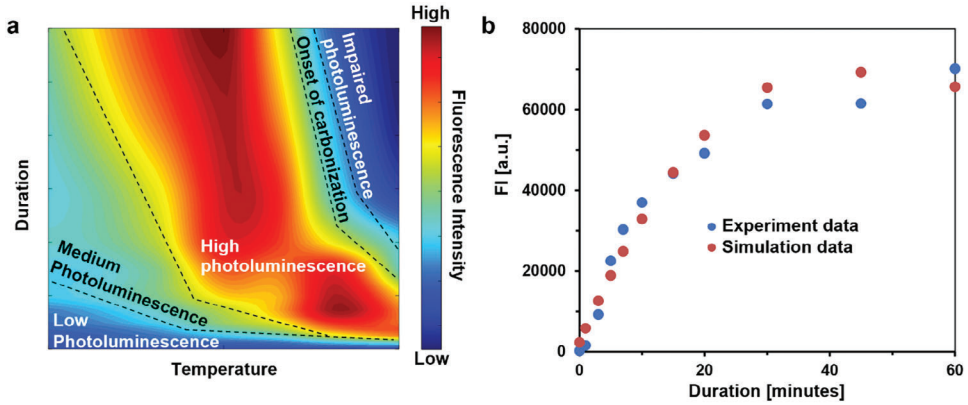

Figure 6. Tunability of FI of in-situ CQDs. a) Heat map of luminescence with varying treatment temperatures and durations. The broken lines separate different FI levels (low, medium, and high). FI was found to initially increase with heating durations and higher temperatures. However, beyond a heating dosage (10 min and 230 °C), excessive carbonization of paper starts, resulting in attenuated luminescence. b) Comparison between experimental and simulation data using a nucleation-growth model (Prout-Tompkins rate equation).

reactions, various chemical pathways, formation of unstable intermediates, and both heat and mass transfers.[58] As seen in the fluorescence Intensity (FI) heat map in **Figure 6a**, luminescence of the in-situ CQDs was highly dependent on the heating parameters. A minimal threshold setting of 150 °C for 20 min was required to initiate the CQDs formation process, where the magnitude of fluorescence was observed to be proportional to the amount of energy transferred. Cellulose heat-treated under different heating conditions showed differences in the peak FI but not in the compounds formed based on elemental analyses. FI peaked at moderate temperatures and moderate-to-high durations. At higher treatment dosages (exceeding 10 min of heating at temperatures exceeding 230 °C), excessive carbonization of the paper substrate resulted in a marked attenuation in the FI.[59] A previous study has described the pyrolysis of cellulose using a nucleation-growth model (Figure S11, Supporting Information) adhering to the Prout-Tompkins rate equation.[60] Using the model, we were able to fit our experimental data with a near complete overlap (Figure 6b), suggesting that the identity of the CQDs is primarily the pyrolysis residues rather than the other byproducts (oligomers, sugars, furans and acids). These findings suggest that the duration and temperature of the heat treatment are critical parameters governing the formation of CQDs without ablating the paper. This allows for the optimization of the CQD fabrication protocol to maximize fluorescence yield and minimize fabrication resource consumption. This heat map would be essential in designing a new nano-sensor using CQDs fabricated by our method.

The tunable peak FI may be attributed to two main mechanisms – 1) the size-dependence of the photoluminescence of the synthesized CQDs and 2) the valence electron transition in the molecule. The current relation between the particle size of CQDs and the resultant peak FI illustrates the energy gap within the core. For CQDs with graphitized core, the smaller the size of core, the higher its photoluminescence energy, whereas CQDs with amorphous core show an inverse trend.[61] Since the photoluminescence originates from surface trap sites, smaller CQDs with larger surface-to-volume (or "the number of the trap sites"-to-"the number of the photo-excitable electrons") ratio could exhibit a higher FI at the same λ_{ex},[62] as observed in our CQDs. Our results clearly demonstrate that the heating temperature and duration play a key role in controlling the size of the CQDs.[63] This size-dependence of the FI of CQDs with graphitized cores has also been previously ascribed to a higher abundance of surface luminescent groups on smaller CQDs,[64] resulting in a higher photoluminescence energy density.[61] The peak FI tunability feature combined with the remarkable photostability and solid state in-situ fabrication offer the possibility of developing a novel paper-based, disposable nano-sensor. Furthermore, we demonstrated the reproducibility of the CQD synthesis using two other brands of filter paper (Hawach Scientific, Qualitative Grade, China and Fisher Scientific, Grade P4, USA), both of which yielded CQDs with identical peak excitation and emission wavelengths (Figure S12, Supporting Information).

During blood storage, red blood cells undergo biochemical and biophysical changes that ultimately culminate in pronounced hemolysis, releasing CFH into the suspending medium. CFH is a potent scavenger of nitric oxide, an important endogenous vasodilator. A reduction in nitric oxide bioavailability in microcirculatory networks can have deleterious outcomes such as inadequate organ perfusion, organ injury and eventually organ failure.[65] In current practice, a quality control in blood banks is performed using the sampling method, in which blood units are randomly selected for hemolysis checks. Since this test method is destructive, it is not applicable to all blood units before transfusion.[66] At present, the main routine test to confirm the blood quality prior to transfusion is the visual assessment of hemolysis (color change recognition) by individual clinicians.[67] However, such a visual assessment is highly subjective and has a tendency to overestimate hemolysis, resulting in unnecessary wastage of much needed blood products.[68] This gap in blood storage management indicates an urgent need for a rapid, affordable, accessible, and accurate platform for CFH detection. The CFH measurement performance of our CQDs in Figure 5l confirms that our CQDs are capable of measuring CFH concentrations for monitoring hemolysis levels in stored blood, which would pave the way for the development of contemporary blood bag inventory management protocols.

© 2025 The Author(s). Small published by Wiley-VCH GmbH

5. Conclusion

We present a one-step simple, low cost in-situ fabrication of CQDs on paper utilizing a conventional oven. We have also demonstrated the highly deterministic tunability of the fluorescence intensity (FI) of our CQDs by facile adjustment of heat treatment duration and temperature. Our parametric studies confirmed that by controlling the heating temperature and duration, we can readily modulate the particle size and the FI peaks of CQDs – optimizing the optical sensitivity of the CQDs for applications. To elucidate the role of heat in forming fluorescing CQDs, we analyzed the surface morphology and chemical compositions of the CQDs. To the best of our knowledge, this study provides the most comprehensive study on the surface chemistry of cellulose-derived CQDs, leading to a nano-sensor design criterion. This allows users to explore the functionalization of CQDs for new applications in the future. Unlike conventional synthesis methods of fabricating CQDs, our method supports a rapid and economical manner to embed CQDs on a cellulose, displaying remarkable stability and repeatability. Our CQDs developed in solid phase permits excellent portability and convenience compared to the conventional solution phase. Furthermore, our in-situ CQDs system showed great potential for detection of CFH in blood bags. We combined the advantages of paper-based biosensors and the photoluminescence of CQDs to develop a reagent-free CFH measurement platform that can be introduced into a blood bag for monitoring of hemolysis. The long-term photostability of the in-situ CQDs enables the paper sensor cartridge to be stockpiled to streamline inventory management. We believe that the demonstrated strategy could significantly improve blood bag management in blood banks, introducing a more reliable method for hemolysis assessment of stored blood – which is a critical metric indicative of blood unit quality.

Supporting Information

Supporting Information is available from the Wiley Online Library or from the author.

Acknowledgements

S.P. and J.K.S.T. contributed equally to this work. This research was supported by the Singapore Ministry of Education (MOE) University Research Committee Tier 2 grant MOE-T2EP50121-0015.

Conflict of Interest

The authors declare no conflict of interest.

Data Availability Statement

The data that support the findings of this study are available from the corresponding author upon reasonable request.

Keywords

biosensing, carbon quantum dots, hemoglobin, paper-based analytical devices

Received: June 4, 2024
Revised: December 13, 2024
Published online: February 3, 2025

[1] S. Y. Lim, W. Shen, Z. Gao, *Chem. Soc. Rev.* **2015**, *44*, 362.
[2] L. Bao, C. Liu, Z. L. Zhang, D. W. Pang, *Adv. Mater.* **2015**, *27*, 1663.
[3] X. Yan, X. Cui, L.-S. Li, *J. Am. Chem. Soc.* **2010**, *132*, 5944.
[4] D. B. Shinde, V. K. Pillai, *Chem.–A Eur. J.* **2012**, *18*, 12522.
[5] X. Sun, Z. Liu, K. Welsher, J. T. Robinson, A. Goodwin, S. Zaric, H. Dai, *Nano Res.* **2008**, *1*, 203.
[6] J. Peng, W. Gao, B. K. Gupta, Z. Liu, R. Romero-Aburto, L. Ge, L. Song, L. B. Alemany, X. Zhan, G. Gao, *Nano Lett.* **2012**, *12*, 844.
[7] a) E. Eftekhari, W. Wang, X. Li, A. Nikhil, Z. Wu, R. Klein, I. S. Cole, Q. Li, *Sens. Actuators, B* **2017**, *240*, 204; b) F.-Y. Tian, R.-X. Cheng, Y.-Q. Zhang, Z. Tao, Q.-J. Zhu, *J. Chem.* **2020**, *2020*, 9619461; c) F. Y. Tian, R. X. Cheng, Y. Q. Zhang, Z. Tao, Q. J. Zhu, *Aust. J. Chem.* **2020**, *73*, 1065; d) Q. Wu, F. Tian, W. Chen, J. Wang, B. Lei, *Nanomaterials* **2023**, *13*, 2732.
[8] Y. Liu, X. Tang, M. Deng, Y. Cao, Y. Li, H. Zheng, F. Li, F. Yan, T. Lan, L. Shi, L. Gao, L. Huang, T. Zhu, H. Lin, Y. Bai, D. Qu, X. Huang, F. Qiu, *Microchim. Acta* **2019**, *186*, 140.
[9] P. Lisowski, P. K. Zarzycki, *Chromatographia* **2013**, *76*, 1201.
[10] W. W.-W. Hsiao, T.-N. Le, D. M. Pham, H.-H. Ko, H.-C. Chang, C.-C. Lee, N. Sharma, C.-K. Lee, W.-H. Chiang, *Biosensors* **2021**, *11*, 295.
[11] A. K. Yetisen, M. S. Akram, C. R. Lowe, *Lab Chip* **2013**, *13*, 2210.
[12] S. J. Park, J. Y. Park, J. W. Chung, H. K. Yang, B. K. Moon, S. S. Yi, *Chem. Eng. J.* **2020**, *383*, 123200.
[13] V. L. John, F. Joy, A. J. Kollannoor, K. Joseph, Y. Nair, T. Vinod, *J. Colloid Interface Sci.* **2022**, *617*, 730.
[14] L. Zhu, Y. Yin, C.-F. Wang, S. Chen, *J. Mater. Chem. C* **2013**, *1*, 4925.
[15] Y. Ma, Y. Cen, M. Sohail, G. Xu, F. Wei, M. Shi, X. Xu, Y. Song, Y. Ma, Q. Hu, *ACS Appl. Mater. Interfaces* **2017**, *9*, 33011.
[16] I. Singh, R. Arora, H. Dhiman, R. Pahwa, *Turkish J. Pharmaceut. Sci.* **2018**, *15*, 219.
[17] C. Li, W. Liu, X. Sun, W. Pan, G. Yu, J. Wang, *Sens. Actuators, B* **2018**, *263*, 1.
[18] W. Yang, H. Zhang, J. Lai, X. Peng, Y. Hu, W. Gu, L. Ye, *Carbon* **2018**, *128*, 78.
[19] H. Zheng, Q. Wang, Y. Long, H. Zhang, X. Huang, R. Zhu, *Chem. Commun.* **2011**, *47*, 10650.
[20] Y.-P. Sun, B. Zhou, Y. Lin, W. Wang, K. S. Fernando, P. Pathak, M. J. Meziani, B. A. Harruff, X. Wang, H. Wang, *J. Am. Chem. Soc.* **2006**, *128*, 7756.
[21] L. Wang, W. Li, L. Yin, Y. Liu, H. Guo, J. Lai, Y. Han, G. Li, M. Li, J. Zhang, R. Vajtai, P. M. Ajayan, M. Wu, *Sci. Adv.* **2020**, *6*, eabb6772.
[22] B. Wang, J. Yu, L. Sui, S. Zhu, Z. Tang, B. Yang, S. Lu, *Adv. Sci.* **2021**, *8*, 2001453.
[23] S. Tajik, Z. Dourandish, K. Zhang, H. Beitollahi, Q. V. Le, H. W. Jang, M. Shokouhimehr, *RSC Adv.* **2020**, *10*, 15406.
[24] Y. Lou, X. Hao, L. Liao, K. Zhang, S. Chen, Z. Li, J. Ou, A. Qin, Z. Li, *Nano Select* **2021**, *2*, 1117.
[25] a) K. Rajendran, G. Rajendran, J. Kasthuri, K. Kathiravan, N. Rajendiran, *ChemistrySelect* **2019**, *4*, 13668; b) Z. Wang, H. Zeng, L. Sun, *J. Mater. Chem. C* **2015**, *3*, 1157.
[26] H. Li, X. He, Y. Liu, H. Yu, Z. Kang, S.-T. Lee, *Mater. Res. Bull.* **2011**, *46*, 147.
[27] M. A. Mohamed, J. Jaafar, A. Ismail, M. Othman, M. Rahman, *Membrane Characterization*, Elsevier, Amsterdam, Netherlands **2017**.
[28] Q. Liu, N. Zhang, H. Shi, W. Ji, X. Guo, W. Yuan, Q. Hu, *New J. Chem.* **2018**, *42*, 3097.
[29] Y. Yang, Y. Zhang, Y. Lang, M. Yu, *IOP Conf. Ser.: Mater. Sci. Eng.* **2017**, *13*, 012039.

 © 2025 The Author(s). Small published by Wiley-VCH GmbH

[30] K. Radhakrishnan, P. Panneerselvam, M. Marieeswaran, *Anal. Methods* **2019**, *11*, 490.
[31] S. Eichhorn, M. Hughes, R. Snell, L. Mott, *J. Mater. Sci. Lett.* **2000**, *19*, 721.
[32] J. De Gelder, K. De Gussem, P. Vandenabeele, L. Moens, *J. Raman Spectroscopy* **2007**, *38*, 1133.
[33] P. Zuo, X. Lu, Z. Sun, Y. Guo, H. He, *Microchim. Acta* **2016**, *183*, 519.
[34] K. J. Mintz, Y. Zhou, R. M. Leblanc, *Nanoscale* **2019**, *11*, 4634.
[35] Q. Li, M. Zhou, M. Yang, Q. Yang, Z. Zhang, J. Shi, *Nat. Commun.* **2018**, *9*, 1.
[36] B. Chen, F. Li, L. Zou, D. Chen, *J. Colloid Interface Sci.* **2019**, *534*, 381.
[37] X. Feng, Y. Xie, W. Zhao, M. Green, L. Liu, X. Chen, *Spectroscopy* **2021**, *36*, 31.
[38] G. S. Das, J. P. Shim, A. Bhatnagar, K. M. Tripathi, T. Kim, *Sci. Rep.* **2019**, *9*, 1.
[39] H. R., *Egyptian J. Archaeologic. Restorat. Studies* **2016**, *6*, 71.
[40] P.-C. Hsu, P.-C. Chen, C.-M. Ou, H.-Y. Chang, H.-T. Chang, *J. Mater. Chem. B* **2013**, *1*, 1774.
[41] P.-C. Hsu, Z.-Y. Shih, C.-H. Lee, H.-T. Chang, *Green Chem.* **2012**, *14*, 917.
[42] V. F. Fairbanks, S. C. Ziesmer, P. C. O'Brien, *Clin. Chem.* **1992**, *38*, 132.
[43] T. W. Yeo, D. A. Lampah, E. Tjitra, R. Gitawati, E. Kenangalem, K. Piera, D. L. Granger, B. K. Lopansri, J. B. Weinberg, R. N. Price, *The J. Infectious Diseases* **2009**, *200*, 1522.
[44] T. T. Bui, S.-Y. Park, *Green Chem.* **2016**, *18*, 4245.
[45] S. Zhu, Q. Meng, L. Wang, J. Zhang, Y. Song, H. Jin, K. Zhang, H. Sun, H. Wang, B. Yang, *Angew. Chem.* **2013**, *125*, 4045.
[46] P. Roy, P.-C. Chen, A. P. Periasamy, Y.-N. Chen, H.-T. Chang, *Mater. Today* **2015**, *18*, 447.
[47] V. Gupta, N. Chaudhary, R. Srivastava, G. D. Sharma, R. Bhardwaj, S. Chand, *J. Am. Chem. Soc.* **2011**, *133*, 9960.
[48] D. Giavarina, *Biochem. Med.: Biochem. Med.* **2015**, *25*, 141.
[49] I. C. V. Windsant, N. C. de Wit, J. T. Sertorio, E. A. Beckers, J. E. Tanus-Santos, M. J. Jacobs, W. A. Buurman, *Crit. Care* **2012**, *16*, 1.
[50] A. A. o. B. B. C. o. Standards, A. A. o. B. B. S. P. Committee, *Standards for Blood Banks and Transfusion Services*, American Association of Blood Banks, Bethesda **1974**, Vol. *41*.
[51] S. H. Arif, N. Yadav, S. Rehman, G. Mehdi, *Indian J. Hematol. Blood Transfus.* **2017**, *33*, 598.
[52] a) Y. Zhang, P. Zhuo, H. Yin, Y. Fan, J. Zhang, X. Liu, Z. Chen, *ACS Appl. Mater. Interfaces* **2019**, *11*, 24395; b) C. Kang, S. Tao, F. Yang, B. Yang, *Aggregate* **2022**, *3*, e169.
[53] Y. Chen, M. Zheng, Y. Xiao, H. Dong, H. Zhang, J. Zhuang, H. Hu, B. Lei, Y. Liu, *Adv. Mater.* **2016**, *28*, 312.
[54] Y. Guo, Q. Wang, H. Li, Y. Gao, X. Xu, B. Tang, Y. Wang, B. Yang, Y.-K. Lee, P. J. French, *ACS Nano* **2022**, *16*, 2910.
[55] Y. Guo, Z. Wang, H. Shao, X. Jiang, *Carbon* **2013**, *52*, 583.
[56] A. V. Bridgwater, *Biomass Bioenergy* **2012**, *38*, 68.
[57] H. Kawamoto, M. Murayama, S. Saka, *J. Wood Sci.* **2003**, *49*, 469.
[58] Y.-C. Lin, J. Cho, G. A. Tompsett, P. R. Westmoreland, G. W. Huber, *J. Phys. Chem. C* **2009**, *113*, 20097.
[59] X. Wang, L. Xu, S. Ge, S. Y. Foong, R. K. Liew, W. W. F. Chong, M. Verma, M. Naushad, Y.-K. Park, S. S. Lam, *Energy* **2023**, *274*, 127354.
[60] N. Paksung, J. Pfersich, P. J. Arauzo, D. Jung, A. Kruse, *ACS omega* **2020**, *5*, 12210.
[61] D. Xu, Q. Lin, H. T. Chang, *Small Methods* **2020**, *4*, 1900387.
[62] W. Kwon, S.-W. Rhee, *Chem. Commun.* **2012**, *48*, 5256.
[63] N. Javed, D. M. O'Carroll, *Nanoscale Adv.* **2021**, *3*, 182.
[64] Q.-L. Zhao, Z.-L. Zhang, B.-H. Huang, J. Peng, M. Zhang, D.-W. Pang, *Chem. Commun.* **2008**, *41*, 5116.
[65] C. D. Reiter, X. Wang, J. E. Tanus-Santos, N. Hogg, R. O. Cannon, A. N. Schechter, M. T. Gladwin, *Nat. Med.* **2002**, *8*, 1383.
[66] J. R. Hess, R. L. Sparrow, P. F. Van Der Meer, J. P. Acker, R. A. Cardigan, D. V. Devine, *Transfusion* **2009**, *49*, 2599.
[67] P. Schlenke, W. Sibrowski, *Transfus. Med. Hemother.* **2009**, *36*, 351.
[68] K. A. Janatpour, T. Paglieroni, V. Crocker, D. DuBois, P. Holland, *Transfusion* **2004**, *44*, 984.

 © 2025 The Author(s). Small published by Wiley-VCH GmbH